A precise, general, non-invasive and automatic speed estimation method for MCSA diagnosis and efficiency estimation of induction motors

Jorge Bonet-Jara, and Joan Pons-Llinares, *Member, IEEE,*

***Abstract*—Efficiency estimation and diagnosis via MCSA require precise knowledge of speed. In an industrial environment, speed must be obtained with a non-invasive, automatic and general method. Recent studies have shown that Sensorless Speed Estimation techniques based on detecting Rotational Frequency Sideband Harmonics (RFSHs) or Rotor Slot Harmonics (RSHs) are best suited to these purposes. RFSHs-based methods are easier to apply as they only depend on the number of poles. RSHs-based are much more accurate due to their wider bandwidth. Yet, their use is not trivial as they require to identify the RSHs family, assign to each RSH its order of the current harmonic (ν) and determine the number of rotor slots (R), a rarely known parameter. This paper ends with this trade-off between accuracy and applicability by proposing a novel RSHs-based technique that, for the first time in technical literature, eliminates the need to estimate the number of rotor slots and provides a reliable and automatic procedure to locate the RSHs family and determine their ν indices. Finally, the method is validated under all types of conditions and motor designs, by simulations, lab tests and with 105 industrial motors, highlighting its high accuracy (errors below 0.05 rpm), and applicability.**

***Index Terms*—Diagnosis, Induction Motors, MCSA, Sensorless Speed Estimation, Efficiency Estimation**

I. Introduction

THERE are two key points when operating induction motors (IM) in industry: maintenance (to avoid untimely outages) and efficiency estimation (to minimize energy consumption). In order to estimate the efficiency it is necessary to measure voltages and currents [1]. Thus, a natural step is to use the same current sensor to diagnose the motor via MCSA (Motor Current Signature Analysis); compared with others, this technique is best suited to this industry context due to its non-invasiveness and remote measurement capability [2]. Moreover, both processes need very accurate speed information [3], [4]. To facilitate the industrial use, the speed must be obtained with a non-invasive and automatic (no-human intervention) method, valid for any IM.

Determining efficiency with good accuracy requires precise operating speed information (e.g., AGT or ORMEL96 [5]). In turn, speed is also vital to localize fault harmonics in the current spectrum, since they are speed-dependent [6]. In fact, speed estimation is the bottleneck of the diagnostic process: a reliable diagnosis requires a previous correct fault harmonic positioning. Some authors propose locating the fault harmonics without knowing the operating speed by calculating the maximum of the spectrum in the harmonic operating bandwidth (determined by the slip varying from 0 to its rated value) [7], [8] . Nevertheless, constructional characteristics, supply, load-oscillations, etc. might generate significant harmonics in these search bands, and produce false positives [9]. Moreover, the fault harmonic might be outside the search band due to an error in the name-plate rated slip, generating a false negative. Concluding, accurate speed knowledge is essential to avoid both false positives and negatives, and therefore, to conduct a reliable diagnosis via MCSA [6], [9].

A physical speed sensor (e.g., encoder) requires a precise and careful assembly and has a cost proportional to its accuracy. In addition, it is sensitive to the operation and location conditions (temperature, cable length, etc.). Finally, manual measurements with hand-held sensors (e.g. tachometers), apart from not being sufficiently accurate, require the shaft to be accessible, which is not always the case. Therefore, giving these limitations, a Sensorless Speed Estimation (SSE) becomes a better option. These techniques (traditionally developed for electric motor control [10]), can be classified into two major families: Fundamental Model Based [11]–[13] and Magnetic Anisotropy Based. The latter can be subdivided into: Signal Injection Based [14]–[16] and Slotting and Rotational Frequency Sideband Harmonics Based (SRFSHB) [17]–[36].

SRFSHB methods are the most suitable for in-service IM efficiency estimation [3] and IM diagnosis via MCSA [4], as they only need to measure one current, do not depend on time-varying parameters (as fundamental model methods do) and do not need the machine to be excited with a source other than its normal power supply (as signal injection methods do). These methods consist of processing the line current in order to determine the frequency of one or more speed-dependent harmonics, and then, using the formulas that predict their frequencies, calculate slip [37]. Rotational Frequency Sideband Harmonics (RFSHs) and Rotor Slot Harmonics (RSHs) are commonly used in these techniques, although sometimes Broken Bar Harmonics (BBHs) may be a complement.

Since they only require the number of pole pairs (available on the nameplate), RFSHs-based methods are preferred by industry, being frequently used in online condition monitoring [20], in-situ efficiency estimation [17]–[19], and commercial diagnostic devices (MCEMAX [21], EXP4000 [22]). However, their frequencies only vary a few fractions of hertz from no to full load [38]. Therefore, a small error in their frequencies estimation implies a large error in the speed estimation. More-

J. Bonet-Jara, and J. Pons-Llinares are with the Instituto Tecnológico de la Energía, Universitat Politècnica de València, C/Camino de Vera s/n, 46022, València, Spain (e-mail: jorboja@die.upv.es; jpons@die.upv.es).

over, they usually encounter detectability problems, especially in 2-pole machines [4].

RSHs-based methods are much more accurate due to their wider operating bandwidth [3], [4]. Yet, using these harmonics is not trivial. The first problem is to identify which harmonics in the spectrum constitute a RSHs family. Then, even assuming that they have been correctly identified, they must be assigned a ν index; there is an erroneous trend to assign $+1$ or -1 to the RSH with the highest amplitude. Finally, to estimate speed, the number of rotor bars (R) must be known. This is a problem, as motor owners are rarely aware of this parameter. Therefore, the applicability of this technique as a non-invasive method is dramatically reduced outside laboratory.

No method has yet solved the problems of this technique in a robust and reliable way. Most of the papers assume R, the position of the RSH in the spectrum and their ν values as known information [23]–[29]. To solve this lack of data, others propose non-automatic/invasive methods that require visual inspection and/or subject the motor to different operating conditions [30]–[33]. Finally, only three papers propose self-commission methods to ascertain this set [34]–[36]:

The method presented in [34], which relies on a preliminary slip estimation from RFSHs, has three disadvantages. First, R is constrained from 30 to 54, which leaves quite a few machines out below 30 (2-pole and small-medium 4-pole machines) and above 54 (medium-large 4-pole and 6-pole machines). Second, RFSHs are an unreliable source of information since small errors in frequency estimation mean big errors in speed. Finally, RFSHs do not often manifest themselves with sufficient intensity to be distinguished from the noise level (especially in 2-pole machines). When this happens, the paper proposes to perform a no-load test to determine the main RSH and asks the user to introduce R (increasing invasiveness and decreasing automaticity).

In [35], the method searches a RFSH and the RSH with $\nu = 1$ (not specifying how the bands are defined). Then, using these two harmonics and the value of the fundamental frequency, R is calculated. If the decimal of R is lower than 0.1 or higher than 0.9, the number is rounded and the process ends; otherwise, the process is repeated (it is not specified how the band for the RSH is re-defined). The drawbacks of this method are the same as in [34] with respect to RFSHs, with the added disadvantage of assuming that RSH ($\nu = 1$) may always be identified automatically .

In [36], the method, which relies on a preliminary speed estimation based on nameplate data, has three disadvantages. First, as stated before, constraining the number of R to test may leave some motors out of the algorithm's scope. Although in this case the range is wider than in [34], large motors could still be left out. Another problem with this methodology, is that it uses a fixed band to localize RSHs (8.609 Hz), which could left some of them out of the window. Finally, the main problem is that the convergence criteria is based on a preliminary speed estimation from nameplate. This estimation can be quite unreliable because nameplate data, apart from being subjected to wide tolerances (especially rated slip), can change through time due to degradation.

Summarizing, RSHs-based methods are preferable due to their high accuracy. Nevertheless, no existing method has solved their low applicability: number of rotor slots needed is unknown, as well as the RSHs position in the spectrum, together with their ν indices. Trying to solve this lack of information, previous methods have proposed problematic solutions. Moreover, reliability is low for existing methods, since among all the RSHs, they only use the so called Principal Slot Harmonics (PSHs), which have low amplitudes for certain motor designs [38]. Finally, SSE methods presented have a poor validation: few laboratory motors (one to four with similar characteristics), and none industrial cases, not ensuring a high reliability.

Concluding, a new SSE method is needed, solving the RSHs-based methods drawbacks, to profit their accuracy necessary in diagnosis and efficiency estimation applications. This is the first SSE method which achieves to automatically localize the family of RSHs, properly assigning their ν indices, without knowing the number of rotor slots, without introducing errors as a preliminary estimate based on rated slip or use of RFSHs, without using invasive tests (e.g., no-load test), not restricting to PSHs, and not wrongly assuming that the highest amplitude corresponds to $\nu = 1$. To this end, a new formula for the RSHs frequencies is deducted, and a smart RSH search method is presented, to localize and characterize the RSHs family (Sections II, III and IV). The algorithm has been extensively tested, not only through simulations (Section V), lab tests under different load conditions and power supply (Section VI), but also through 105 field cases (covering all ranges of rated magnitudes), highlighting the high applicability of the proposed methodology (Section VII). The algorithm provides a SSE easy to be implemented in an industrial environment for IM steady state diagnosis via MCSA and in-situ efficiency estimation, which ends with the trade-off between accuracy, applicability and reliability of previous techniques.

II. Determining RSHs parameters

The discrete nature of the squirrel cage bars causes the rotor to generate magnetomotive force spatial harmonics as well as a periodic variation of the air-gap permeance. By interacting, they produce air-gap flux components which induce in the stator currents a set of speed-dependent harmonics called Rotor Slot Harmonics (RSHs). The relationship between the frequencies of these harmonics and the machine characteristics has been extensively studied [37], [38] and can be given by:

$$f_{RSH} = \left[k\frac{R}{p}(1-s) \pm \nu \right] f_0 \tag{1}$$

where k is a natural number $1, 2 \ldots$, p the number of pole pairs, s the slip, ν the orders of the time harmonics present in the stator current $1, 3, 5 \ldots$, f_0 the fundamental supply frequency and R the number of rotor slots.

Formula (1) depends on the slip, which is directly related with rotor speed. Therefore, once a RSH is localized, if the other parameters in (1) are known, speed can be calculated. The number of pole pairs p and the fundamental frequency f_0 are obtained respectively from the nameplate and a FFT analysis (as f_0 is the highest peak in the spectrum). On the

contrary, the number of rotor bars is an a priori unknown parameter: it is not listed on the nameplate or in the data sheet, nor can it be easily obtained from the manufacturer. Thus, to obtain an automatic, non-invasive, general and precise speed estimation algorithm, it is necessary to eliminate this parameter from the equation. To this end, let us first eliminate $\pm$ sign in (1), so now $\nu = \ldots, -3, -1, 1, 3, \ldots$, and rewrite it as follows:

$$f_{RSH} = \left[k\frac{R}{p} + \nu\right] f_0 - k\frac{R}{p} s f_0 \tag{2}$$

Next, consider the case of ideal no-load ($s = 0$):

$$f_{RSH}|_{s=0} = \left[k\frac{R}{p} + \nu\right] f_0 \tag{3}$$

Then, let us define O_ν, (where the subscript refers to the value of ν taken), as the quotient between the frequency of the RSH at zero slip and the frequency of the fundamental component:

$$O_\nu = \frac{f_{RSH}|_{s=0}}{f_0} = \left[k\frac{R}{p} + \nu\right] \tag{4}$$

Combining (2) and (4) we obtain:

$$f_{RSH} = O_\nu f_0 - [O_\nu - \nu]\, s f_0 \tag{5}$$

Therefore, we can finally calculate the slip as:

$$s = \frac{O_\nu f_0 - f_{RSH}}{[O_\nu - \nu]\, f_0} \tag{6}$$

RSHs only exhibit high amplitude in the stator current spectrum when the product kR/p is even [38]. If an odd number (ν) is added to or subtracted from this product, the result ($O_\nu = kR/p + \nu$) is always an odd number. Therefore, according to (5), the following rule can be established: in ideal no-load ($s = 0$) the most detectable RSHs are placed over an odd multiple of the fundamental frequency ($O_\nu f_0$), while in load, to its left (motor mode, $s > 0$), or to its right (generator mode, $s < 0$).

Taking into account the above rule, once a RSH has been localized in the spectrum, the odd multiple of the fundamental frequency closest to its right (motor mode) is $O_\nu f_0$: knowing f_0, O_ν can be calculated. Therefore, as the number of rotor bars has been eliminated in (6), it only remains to obtain ν for each RSH localized. Next, a novel method based on the steady-state current is proposed to localize the RSHs and determine their related ν.

A. Localizing the RSHs

According to (2) and (5), the distance of a RSH with respect to $O_\nu f_0$ is ksf_0R/p. R/p is constant and sf_0 (slip frequency) is the same for all RSHs. Therefore, if a set of RSHs are linked to the same k, all remain at the same distance (in Hz) from their respective $O_\nu f_0$. Let us define such set as a family of RSHs. Figure 1 shows three fragments of the stator current spectrum from a 248 kW IM where three RSHs are shown at the same distance (31.10 Hz) from the first odd multiple of f_0 at their right, thereby belonging to the same RSHs family. Considering this rule, the following Track & Find algorithm has been developed to localize a RSHs family (small clarifications in the next paragraph):

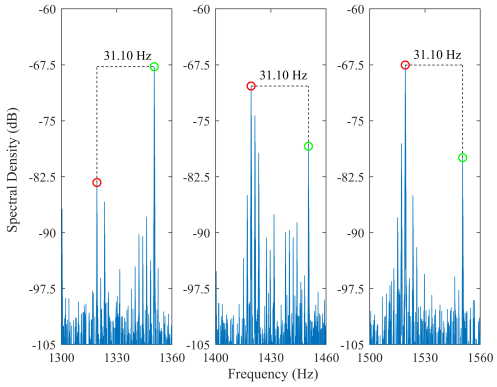

Fig. 1. Distance between the RSHs of a same family (red circles) and their nearest odd multiple of f_0 (green circles) in the steady-state current of a 248 kW IM. From left to right: RSH(-3), RSH(-1) and RSH(+1).

- *Step 1:* The FFT spectrum of the line current is subdivided in windows of width $[f_0 \cdot (2n-1), f_0 \cdot (2n+1)]$ Hz (starting at $n = 4$, until it is entirely covered).
- *Step 2:* The widths of the windows are slightly reduced by subtracting 1.3 Hz to the upper limit and by adding $0.26 \cdot f_0$ to the lower.
- *Step 3:* The frequency of the highest peak within each window is recorded as a RSH candidate.
- *Step 4:* The RSH candidates are classified by families. Two candidates belong to the same family if they are at the same distance (with a tolerance of 0.5 Hz) from the upper limit (lower if generator mode) of their search window (the correspondent $O_\nu f_0$).
- *Step 5:* The family with the highest number of candidates is selected as a possible RSHs family. In case of a tie, all the tied families are selected.

In *Step 1*, n starts at 4 since RSHs are not expected to be found in windows with $n < 4$, given that a motor is normally made with $R/p > 10$. In *Step 2*, windows are reduced in order to avoid capturing odd multiples of f_0, as well as other harmonics that appear near them (e.g, Dynamic Eccentricity Harmonics (DEH)). The reduction parameters are determined experimentally and verified through a motor database of 105 IMs of different rated powers (see Section VII). Finally, in *Step 4*, the tolerance is also established empirically and accounts for slight speed variations during the signal capture.

B. Determining the parameter ν

Once the candidates RSHs families have been detected, it is necessary to determine the parameter ν of each RSH candidate. Here, an iterative method is proposed, whose convergence criteria is based on the information provided by 16 different speed-dependent harmonics (frequency formulas in Appendix A): BBHs first ($k = 1$ and $k = 2$) and second family ($k/p = 5$ and $k/p = 7$), RFSHs ($k = 1$ and $k = 2$) and DEHs ($n_D = 1$). To improve the effectiveness in low-slip motors, the BBHs ($k = 1$ and $k = 2$) present in the spectrum of the current Hilbert modulus are also included [39].

Next, the method for determining ν is described. This process is repeated for each RSH candidate of each family:

- *Step 1:* O_ν is calculated as explained in Section II.
- *Step 2:* A value for ν is selected, beginning in -27 and ending in $O_\nu - 10$, and the following process is applied for each of these values:
  - *Step 2.1:* s is obtained from (6), using the calculated O_ν, the selected ν and the RSH candidate frequency.
  - *Step 2.2:* A frequency window is calculated for each harmonic considered in Appendix A using $[0.75s, 1.25s]$.
  - *Step 2.3:* The frequency of the highest peak within each window is recorded.
  - *Step 2.4:* If the distance between the highest peak and the centre of the window is less than 7% of the window amplitude, the tested value for ν is considered to correctly locate the correspondent fault harmonic.
- *Step 3:* The ν finally assigned to a given RSH candidate is the one that has correctly located (according to *Step 2.4* criteria) the largest number of fault harmonics (in case of a tie, the lowest ν is chosen).

Up to this point, each RSH candidate of each family has been assigned a pair [O_ν, ν]. Two RSH candidates are consistent if when applying $kR/p = O_\nu - \nu$ they give the same result. The most repeated kR/p in a candidate RSHs family is obtained, and the percentage of RSH leading to that value is called the consistency ratio of that family. This concept is used in the following validation process to discard the candidate families that are unlikely to be the RSHs family:

- *Step 4:* If one of the RSHs in a family fails to predict the position of all the fault harmonics for all ν, the whole family is discarded.
- *Step 5:* Consistency ratio is calculated as previously defined: if it is less than 50%, the whole family is discarded.
- *Step 6:* Finally, the family with the highest consistency ratio is selected as the definitive RSHs family; its inconsistent RSHs are discarded and the consistent stored.

In *Step 2*, the set of values for ν is empirically determined using the 105 IM database (see Section VII): it has never been found a ν index lower than -27 or greater than $O_\nu - 10$ (this would mean a motor with less than 10 R/p). In *Step 2.4*, the 7% margin accounts for speed variations during recording as well as for the frequency resolution error. In Hz, this margin is very small: e.g., between 0.01 and 0.05 Hz for the LSH of a motor with $R/p = 28$).

Among other important advantages, summarized in the conclusions section, at this point it can already be seen how the algorithm manages to perform a SSE without knowing the rotor slots, automatically localizing the RSHs family in the spectrum, and assigning their related O_ν and ν indices. It works without any restriction (general solution), even for motors not Principal Slot Harmonics (PSH) producers (RSHs with $k = 1$, [38]), since it also accounts for $k > 1$ in (1), and without using invasive procedures (just a steady state current). The algorithm result assures a perfect match between the slip information of the speed-dependent harmonics present in the current spectrum (RSHs and fault harmonics, which also appear in healthy conditions, as all motors have a certain level of electrical and constructive asymmetry). In other words, thanks to the novel criterion introduced, it is verified that the slip predicted by the RSHs agrees with the position of the remaining speed-dependent harmonics.

TABLE I
ORDERS k OF RSHS FOR EACH COMBINATION OF R AND p

	$p = 1$	$p = 2$	$p = 3$
R even	$\forall k \in \mathbb{N}$	$\forall k \in \mathbb{N}$ if $R/4 \in \mathbb{N}$ k even if $R/4 \notin \mathbb{N}$	$\forall k \in \mathbb{N}$ if $R/6 \in \mathbb{N}$ $k/3 \in \mathbb{N}$ if $R/6 \notin \mathbb{N}$
R odd	k even	$k/4 \in \mathbb{N}$	k even if $R/3 \in \mathbb{N}$ $k/6 \in \mathbb{N}$ if $R/3 \notin \mathbb{N}$

III. ON THE ORDER k OF THE RSHS

The order k of the RSHs present in the spectrum depends on the number of rotor slots R and pole pairs p: kR/p must be even for a RSH of order k to appear. This condition leads to Table I, which shows the orders k that appear for each combination of R and p (where $R/a \in \mathbb{N}$ means R can be divided by a, giving as a result an integer).

The most critical cases for the algorithm are those combinations which produce RSHs families whose minimum order k is a high number, since these harmonics tend to have a lower amplitude. Looking at the table, those cases are motors with $p = 2$ and R odd ($k_{min} = 4$) and motors with $p = 3$ and R odd number non-multiple of 3 ($k_{min} = 6$). Yet, manufacturers usually avoid odd numbers for R (especially if $kR/p \notin \mathbb{N}$ as in these cases), due to the appearance of unbalanced magnetic pull [40]. In fact, when analyzing the database contained in [41] with data about R and p of 3474 motors with $p = 1$, 2 and 3, these two cases account only for the 5.33% and 3.2% respectively.

Nevertheless, even if analyzing a motor without RSHs of orders $k = 1, 2$, and 3 is an uncommon case, in Section V it can be seen how the algorithm successfully detects the RSHs in a motor whose first appearing order is $k = 4$. As previously stated, every RSH operates at the left of some odd multiple of the fundamental component. According to (3), the frequency of this multiple increases with the order k of the RSH. However, this makes no difference for the algorithm, since it searches in a bandwidth to the left of every odd multiple of f_0, no matter if they are at low or high frequencies. Therefore, if the minimum RSH order k present in the motor is for instance 4, it means that the first RSHs will be found at higher frequencies than those of $k = 1$ if they were also present, but the behavior of the algorithm is exactly the same. Although for higher k the amplitudes are lower, it is also true that they appear at higher frequencies, where there are less components with which they can be confused. Hence, the algorithm can also work well in these conditions.

Finally, it is also interesting to analyze what would happen if the frequency operation bandwidth of two RSHs of different order k overlap. To this end, let us consider two RSHs defined by $[k_1, \nu_1]$ and $[k_1, \nu_1]$, both operating at the left of: $[kR/p + \nu]f_0$. Therefore, the overlapping condition is $k_1 R/p + \nu_1 = k_2 R/p + \nu_2$. If $k_1 = 1$ and $k_2 = 2$, then $\nu_1 - \nu_2 = R/p$. In

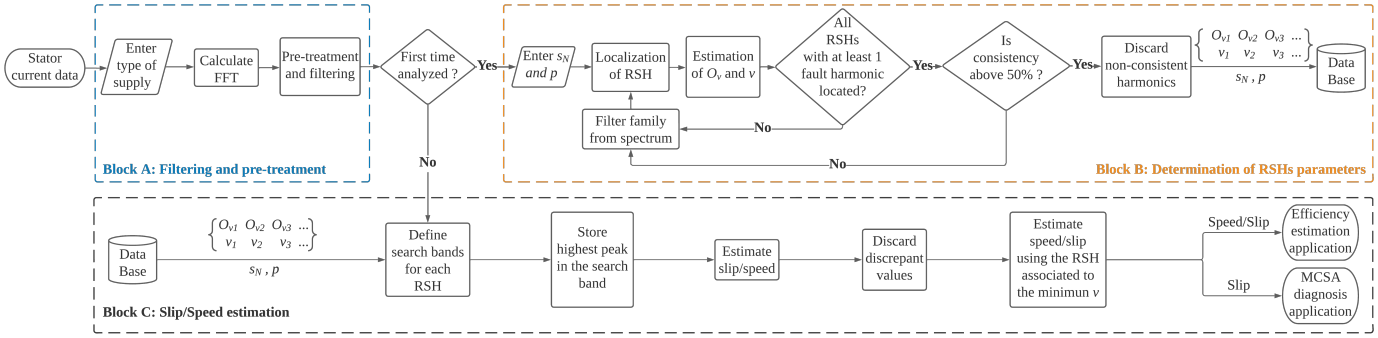

Fig. 2. Flux diagram of the proposed algorithm.

the database of [41], it is found that the minimum R/p is 9, that only 3.2% of the motors have $R/p < 14$, and that 68% of them have $R/p > 20$ (for powers greater than 100 HP, all $R/p > 15$). Therefore, the absolute value of ν_1 and ν_2 will unlikely be simultaneously small, since their difference (R/p) is usually high (most of the cases higher than 14). Since high RSHs amplitudes are usually related to low absolute values of ν, it is unlikely that two RSHs whose bandwidths overlap have simultaneously high amplitudes (one of them will probably be negligible).

Nevertheless, if both RSHs are not negligible, the algorithm will choose the one with the highest amplitude, determine its distance to the nearest odd multiple of f_0 and put it into the family associated to that distance. The second RSH will be discarded, and its family will lose a member, decreasing its chances to be chosen to determine the speed. Concluding, if two valid families of RSHs coexist in the spectrum, both can be used to determine the speed (algorithm picks the one with the highest number of RSHs), and makes no difference if the algorithm discards one RSH in a bandwidth in which two RSHs of different families can be found.

IV. Algorithm

Figure 2 depicts the flux diagram of the proposed technique. As can be seen, the methodology is characterized by three different blocks: Filtering and pre-treatment (Block A), Determination of RSHs parameters (Block B) and Slip/Speed Estimation (Block C). For the sake of simplicity, Block B has been represented for the case in which only one RSHs family is proposed as a candidate at the end of Section II-A. The SSE algorithm has been implemented using MATLAB in a PC with an Intel Core i7-8700 processor. The processing time is 2 s (A+B+C, new motor) or 1.8 s (A+C, already analyzed motor) for a 200 s signal at 10 kHz. Next, the three blocks are described.

A. Block A: Filtering and pre-treatment process

First, the algorithm requires the user to enter whether the motor is powered with a frequency converter or not. Then, the FFT is applied to the current, and to its Hilbert modulus, previously applying Hann window and zero-padding (x10). Next, a pre-treatment and filtering process is applied to the resultant current spectrum (later used to localize the RSHs):

- Estimate the noise level: mean value of the current spectral density multiplied by an experimental factor.
- Suppress harmonics below the estimated noise level.
- Suppress even harmonics of the fundamental frequency.
- If the motor is fed with a frequency converter, suppress the PWM harmonics.

B. Block B: Determination of RSHs parameters

If it is the first time that the motor is analyzed, family of RSHs must be localized, and its pairs $[O_\nu, \nu]$ must be ascertained. For this purpose, it is required to capture a signal of 50 to 200 s (frequency resolution between 0.02 Hz and 0.005 Hz to increase precision) at $200 f_0$ Hz (maximum frequency $100 f_0$ Hz to ensure RSHs detection). The number of pole pairs and the rated slip must be entered as input data. Then, the pairs $[O_\nu, \nu]$ are determined as described in Section II, and finally stored in a database, together with the rated slip and number of pole pairs of the motor.

C. Block C: Slip/Speed estimation

If the motor has already been analyzed (minutes, days or months before), Block B has already been applied with a different current, determining the RSHs family, and their pairs $[O_\nu, \nu]$. In a new measurement, exact position of the RSHs might have changed, since the operating conditions might be different, but their pairs $[O_\nu, \nu]$ are the same. Therefore, using the Block B output contained in the database, a search window is defined for each RSH (see (5)):

$$\begin{aligned} f_{RSH,min} &= O_\nu f_0 - (O_\nu - \nu)\, k_1 s_N f_0 \\ f_{RSH,max} &= O_\nu f_0 - k_2 \end{aligned} \tag{7}$$

where k_1 and k_2 are experimental factors to compensate the tolerance in the rated slip (min) and to avoid detecting an odd multiple of the fundamental (max).

Then, using the frequency of the highest peak in each of these windows and applying (6), slip and speed are estimated. Some of these peaks might not be RSHs, as the feeding and loading conditions might be different from the time when the pairs $[O_\nu, \nu]$ were determined, and therefore, it might happen that some of the RSHs are no longer the highest peak in its search band. Peaks not being RSHs must be detected and discarded. To this end, the algorithm uses a classic criterion for

outlier detection: peaks whose slip/speed estimation are more than three scaled median absolute deviations away from the median of all the slip/speed estimated. Once the outliers are discarded, the slip/speed output is computed using the RSH of the lowest ν, as it provides the lowest error. Furthermore, this Block only requires a current captured at $200f_0$ (to ensure RSHs detection), while duration depends on the precision needed. Finally, it must be remarked that, up to date, the algorithm has been tested for steady state applications; further research will be conducted to prove its use under load oscillations, where a high frequency speed estimation is needed.

V. Simulation

This section proves through simulations the capability of the algorithm to precisely estimate the speed for an arbitrary number of R/p, load level or skewing angle. As stated in Section II, the algorithm is designed to track any RSH predicted by (1). Therefore, even in an IM with an odd or non-integer number of R/p, where RSHs associated to $k = 1$ in (1) are not expected to appear, the algorithm could track those of higher order ($k = 2, 3, 4 \dots$). Nevertheless, the amplitude of these harmonics, and therefore their detectability, decreases with k, apart from being also affected by the load level and the skewing angle of the rotor bars. Therefore, it is important to test the ability of the algorithm to correctly determine the parameters associated with each RSH taking into account all these factors. To do so, the algorithm is input with simulated signals (100 s, 10 kHz) from a model of a 4-pole 4 kW IM (model information can be found in [42]). The rotor of the simulated motor is configured under three different number of bars: 26 (odd R/p), 27 (non-integer R/p) and 28 (even R/p). Then, each configuration is tested under 85% and 55% of the rated load (industrial motors are usually oversized, working usually around 85%, and rarely under 55%). Four typical skewing angles are used: $0°$ (straight bars), $180°/R$ (half rotor slot pitch), $360°/N_{est}$ (one stator slot pitch; N_{est}: stator slots) and $360°/R$ (one rotor slot pitch).

In order to get the simulations as realistic as possible, the model is fed with a real three-phase voltage system measured in an industry. In addition, a white Gaussian noise is added to the resulting simulated currents to have a noise floor similar to reality. Finally, a slight electrical asymmetry is introduced in the rotor (common in industry, as seen in the results of the 105 IM analyzed in Section VII), through increasing the impedance of one of the bars by 10% (this motor needs a 900% increment to obtain a Lower Sideband Harmonic (LSH) with a -37 dB amplitude, which is considered as a broken bar).

The algorithm results are shown in Fig. 3, plotting the number of RSHs detected, for 85% (up) and 55% (down) of the rated load, for different number of bars (26, 27 and 28) and different skewing angles. The algorithm succeeds in 23 out of 24 cases. As explained further below, it fails (no RSH detected) in the case with low load, 26 bars and one rotor slot pitch skewed. In the successful cases (all the rest), the algorithm detects from 2 to 9 RSHs, even under nearly no load situation. The number of RSHs detected decreases when the bars are skewed, being the most severe cases when the bars are skewed one rotor slot pitch.

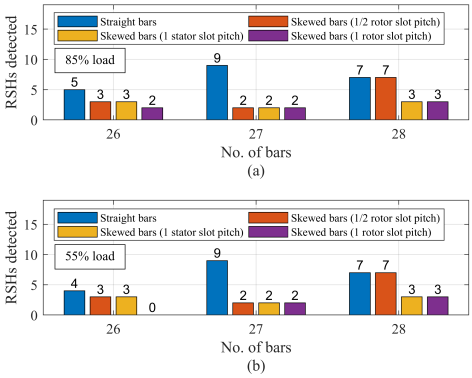

Fig. 3. Number of RSHs detected by the algorithm for different number of rotor bars and skewing angles at two loads: 85% (a) and 55% (b).

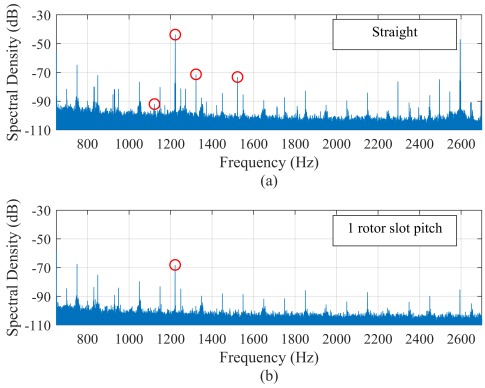

Fig. 4. Detectable RSHs in the configuration of 26 bars at 55% of load with unskewed bars (a) and one rotor slot pitch skewed bars (b).

With 27 and 28 bars, the algorithm detects the RSHs associated with $k = 4$ and $k = 1$ respectively. This is in accordance with theory as $k = 4$ and $k = 1$ are the lowest k for which kR/p is even, for 27 and 28 bars respectively (see Section II).

Similar results are obtained for 26 bars (where the RSHs detected are the ones for $k = 2$), except under 55% of the load, with the bars skewed one rotor slot pitch. This is the only case in which the algorithm fails to detect the RSHs family. Error appears since only one RSH is the highest in its search window, and there are two speed-independent grid harmonics in the spectrum that also satisfy the rule set in Section II-A to be considered a RSHs family. This is caused by the skewing of the bars, which significantly reduces the RSHs amplitude: Fig. 4a (unskewed bars, 4 RSHs detected), Fig. 4b (one rotor slot pitch skewed bars, only 1 RSH detectable). Nevertheless, although skewing of the bars is a common practice in small motors, it is not in large ones, due to the difficulty in the manufacturing process and the increase in the iron losses, which are the most significant in this type of motors [43]. Moreover, in the only case in which the algorithm has failed, the motor works at an extremely low load level, nearly never found in an industrial environment.

Finally, it should be noted that, due to the ideal characteristic

of the model, the number of detectable RSHs is inferior to real motors: the inherent asymmetries, as well as the non-linearity of the iron core, intensify some of the RSHs that are below noise level in the spectrum obtained through the model. In Section VII, it will be shown how the number of detectable RSHs in a database of 105 industrial IM is even superior to the results shown here.

VI. Lab Test

In this section, the algorithm performance is evaluated, using signals from a 2.2 kW IM (28 bars skewed $1/2$ rotor slot pitch, 1420 rpm, 230V Δ), which can be supplied from the grid or from a frequency converter. An identical IM is coupled to its shaft and fed with a second frequency converter, to act as a load. Speed is measured using a 1000-line incremental encoder installed on the shaft end, while current is measured using a current probe (PicoTech TA189). Both signals are simultaneously recorded using an oscilloscope (PicoTech 4262). In order to assess the capabilities of the algorithm in localizing the RSHs, determining their pairs $[O_\nu, \nu]$ (Block B) and obtaining the speed/slip (Block C), three different supply frequencies are used (20 Hz, 35 Hz and 50 Hz-line-fed), with three different slips at each of these frequencies (0.046, 0.02 and 0.0067). For testing Block B, signals of 200 s are used, while for testing Block C, 50 signals of 50 s per case are taken to obtain the average errors in speed and slip. A duration of 50 s is used because it provides the sufficient frequency resolution for a MCSA diagnostic application.

Figure 5a shows, for each of the cases analyzed (20, 35 and 50 Hz-Line-Fed, and three slips at each frequency), the number of RSHs detected: it varies from 5 to 7, which is in accordance with the results shown in the previous section for a motor with bars skewed $1/2$ rotor slot pitch. In this IM, $R/p = 14$ and the pairs $[O_\nu, \nu]$ assigned by the algorithm to the RSHs detected give $kR/p = O_\nu - \nu = 14$. Therefore, the algorithm perfectly detects the RSHs (using those associated to $k = 1$), and their related parameters $[O_\nu, \nu]$. Moreover, the RSHs help to detect from 5 up to 8 fault harmonics (Fig. 5b: number of fault harmonics localized). It is logic to expect a variation in this value depending on the supply frequency and the slip, as fault harmonics can be affected by them. Nevertheless, the value is still high in all cases, showing a good consistency between the slip estimation through RSHs, and the slip-dependent information contained in the spectrum through fault harmonics.

Concluding, the algorithm precisely identifies the RSHs family, and determines its parameters $[O_\nu, \nu]$, even under the most unfavorable conditions, which are a low supply frequency and a low slip. In this situation, some of the harmonics used in the algorithm can appear very near to other relevant harmonics and be masked by them (e.g., BBH near the fundamental frequency or RSHs near winding harmonics). Nevertheless, the fact of using an analysis based on the consistency of the speed information between the RSHs detected and up to 16 different fault harmonics makes it possible for the algorithm to identify the RSHs and resolve the correct values for the pairs $[O_\nu, \nu]$, which perfectly match with the exact number of $kR/p = O_\nu - \nu = 14$ present in the IM.

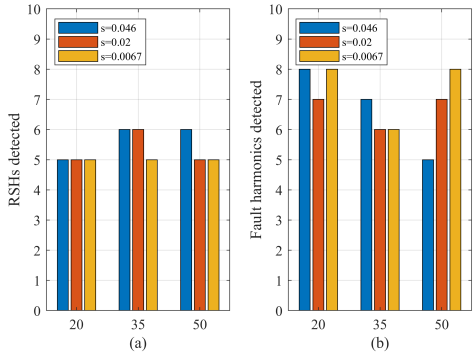

Fig. 5. Number of RSHs (a) and fault harmonics detected (b) for three different supply frequencies (20 Hz, 35 Hz and 50 Hz-Line-Fed) and slips (0.046, 0.02 and 0.0067).

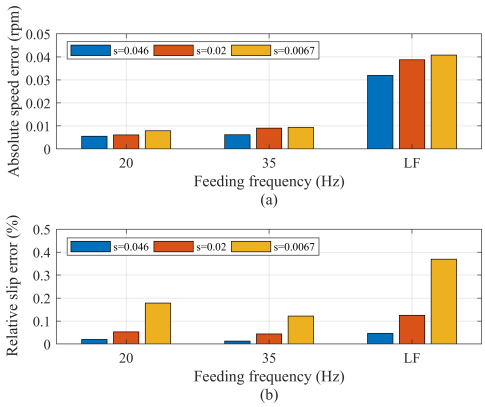

Fig. 6. Absolute speed error (a) and relative slip error (b) for three different supply frequencies (20 Hz, 35Hz and 50 Hz-Line-Fed) and slips (0.046, 0.02 and 0.0067)

Figure 6 shows the absolute speed error (Fig. 6a) and the relative slip error (Fig. 6b) between the 1000-line encoder and the algorithm. Errors are obtained for the three supply frequencies, and for the three slips at each supply frequency. Errors are extremely low in all cases: below 0.05 rpm and 0.5% (if the slip is 1% and the slip relative error is 0.5%, the measured slip is either 1.005% or 0.995%). It should be noted that, as the frequency converter is able to maintain a more stable supply frequency than the grid, the errors are much smaller ($e_{speed} < 0.01$ rpm and $e_{slip} < 0.2\%$) . Finally, errors are especially low under high load, since the load level is influencing the speed stability in this motor, causing the error to increase as the load decreases. The error shown in each case is the average error of 50 signals captured under the same operating conditions. Therefore, the algorithm is highly reliable.

VII. Field Test

In this section, the algorithm is validated using real measurements of 105 industrial IM. All signals have been obtained using an oscilloscope (PicoTech 4824) and a current probe (PicoTech TA167), except for ten motors that were measured

using a device with a limited sampling frequency of 2.6 kHz. Most of the 105 motors have been monitored two or three times, while some of them have been diagnosed every six hours during nearly a year, using this algorithm in the process (results of failure cases presented in [42]).

Figure 7 shows the number of motors in the database for each of the ranges of rated power, slip, voltage and number of pole pairs. As can be seen, the database covers a wide range of different types of motors: from a few kW to 2 MW, 0.67% to 8% slip, 400 V to 6.6 kV and from 1 to 5 pole-pairs. Figure 8 shows the rated slip (y-axis) and the supply frequency (x-axis) for all the motors supplied by the grid (blue circles) and by frequency converters (red circles). In this regard, it should be noted that the algorithm has been tested with a considerable amount of motors with low rated-slips (21 motors with slip lower than 1%), and converter-fed at low frequencies, which are the most challenging conditions for algorithms based on harmonic detection. Therefore, this database is a great tool to validate and demonstrate the high applicability of the proposed method. As for the validation methodology, the following strategy has been followed:

Whenever possible, the speed has been measured and a direct comparison with the speed estimated by the algorithm has been made. Otherwise (e.g, shaft not accessible), a visual inspection of the spectrum has been performed through three steps. First, the RSHs family localized by the algorithm has been identified in the spectrum. Second, it has been checked if there is another significant harmonic family, not detected by the algorithm, that satisfies the rules of Section II for being a RSHs family: harmonics at the same distance of their respective multiple of f_0. Third, a manual determination of parameters O_ν and ν has been conducted for all families accomplishing that rule, verifying that the family and its respective indices O_ν and ν selected by the algorithm are the ones that perfectly match with the rest of speed-dependent harmonics present in the spectrum.

In this regard, after applying the algorithm to the 105 IMs, there are only five of them where it has not been possible to assess whether the results are correct or not. This has been due to the fact that these measures were taken in conditions for which the algorithm is not designed for: high noise-floor (two IMs with -67 dB, while in the rest of motors the value is around -90 to -100 dB), very low load (one IM running at 37% of the rated current) and transient operation (two IMs with significant load variations).

A. Results: three critical examples.

The three figures depicted in this subsection show the RSHs and fault harmonics localized by the algorithm for three different IMs. Subfigures (a) represent the spectrum with the number of RSHs detected (red circles) and the RSH used to estimate speed (black circle), while the rest of subfigures show the estimated position of the most relevant speed-dependent harmonics: the LRFSH (b), the URFSH (c), the first family of BBHs (d) and the second family of BBHs (e), (f).

Figure 9 shows the results for a four-pole, 90 kW IM running with a slip of 0.3% and a supply frequency of 20

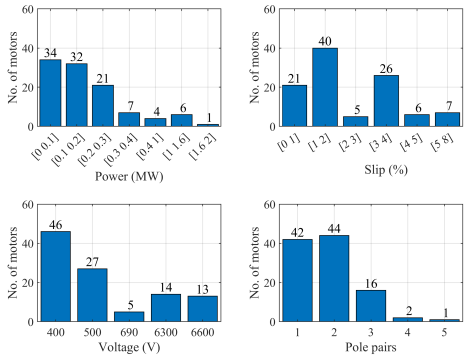

Fig. 7. Summary of the rated characteristics of the motor database.

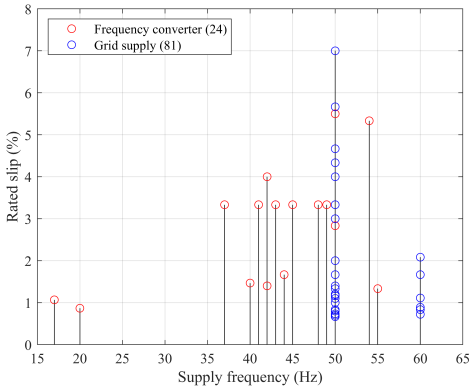

Fig. 8. Rated slip and supply frequency of each motor of the database.

Hz. This is one of the most challenging conditions for the algorithm since the spectrum is highly polluted (affecting the RSHs localization) and the speed-dependent harmonics appear very close to multiples of the fundamental frequency (affecting the estimation of ν). However, the algorithm precisely detects 6 RSHs and 6 fault harmonics localized through them (2 of them shown in Figs. 9b and 9c, 2 in 9d and 1 in 9e).

Figure 10 shows the results for a two-pole, 112 kW, line-fed IM running with a slip of 2.9%. In this case, the algorithm has detected 17 RSHs, which enable to localize 11 fault harmonics (9 of them shown in Figs. 10c, 10d, 10e and 10f). It is worth to remark that, an algorithm based on detecting RFSHs would have failed, since there are two harmonics with a higher amplitude next to them, as shown in Fig. 10 (b) and (c).

Figure 11 shows the results for a two-pole, 172 kW IM running with a slip of 1.5% and a supply frequency of 43.97 Hz. In this case, the spectrum is less polluted than in Fig. 9, so the number of detected RSHs increases to 10, and the number of fault harmonics localized is 8 (all of them shown in Figs. 11d, 11e and 11f). As in the previous case, an algorithm based on detecting RFSHs would have failed, since they are below noise level, as shown in Fig. 11 (b) and (c).

B. Statistical analysis

Figure 12a represents the number of RSHs detected by the algorithm in each of the motors analyzed along with the

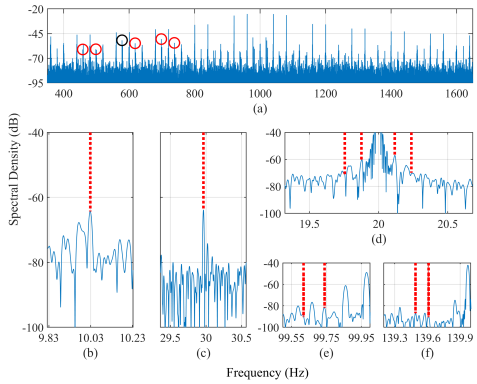

Fig. 9. Algorithm performance in a four-pole 90 kW IM fed at 20 Hz: detected RSHs (a) and location of LRFSH (b), URFSH (c), first family of BBHs (D) and second family of BBHs (e) and (f).

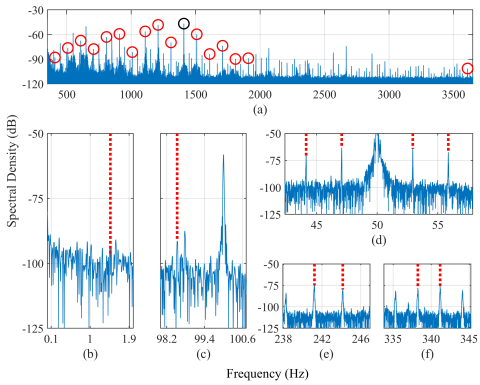

Fig. 10. Algorithm performance in a two-pole 112 kW IM line-fed: detected RSHs (a) and location of LRFSH (b), URFSH (c), first family of BBHs (D) and second family of BBHs (e) and (f).

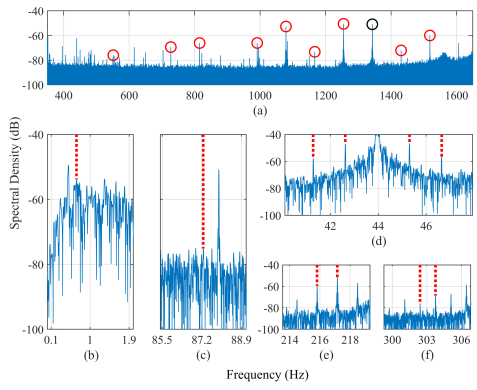

Fig. 11. Algorithm performance in a two-pole 172 kW IM fed at 43.97 Hz: detected RSHs (a) and location of LRFSH (b), URFSH (c), first family of BBHs (D) and second family of BBHs (e) and (f).

final mean and boxplot. According to it, the mean value of detections is 7.3, while the median is 6. It is also worth to remark that in 75% of the cases the number of RSHs detected is more than 4, and that in some cases it can reach values up to 24. Finally, there are 14 cases where the number of detected

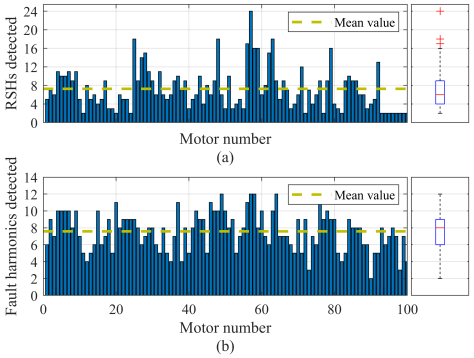

Fig. 12. For each motor of the database: number of RSHs detected (a) and number of fault harmonics properly localized through the RSHs (b).

RSHs is equal to 2. However, 10 of them were measured with a 2.6 kHz sampling frequency. Therefore, it is highly likely that more harmonics would have been detected if the sampling frequency had been $200 f_0$, as in the rest of signals.

Figure 12b represents, for each of the motors analyzed, the number of fault harmonics properly localized through the detected RSHs family. According to it, the mean value for the database is 7.6, the median 8 and the first quartile 6. This gives us a measure on how robust the determination of O_ν and ν has been for all RSHs of the family, since it depicts the degree of coherency between the slip estimated through each RSH using the pair O_ν and ν obtained, and the rest of speed-dependent harmonics considered (fault harmonics).

Concluding, the algorithm has been tested with an extensive and varied database giving a mean value of: 7.3 RSHs detected per motor, and 7.6 average number of fault harmonics localized. These results demonstrate the robustness of the method, since the slips estimated through the RSHs localized and their assigned pairs $[O_\nu, \nu]$ allow locating a high number of speed-dependent fault harmonics, thus verifying the coherence between the estimated O_ν and ν and the information available in the spectrum. Finally, it is also shown that the method is more robust in two-pole machines than those based on detecting RFSHs, as it was confirmed in more detail in [4].

VIII. Conclusions

A new SSE algorithm based on RSHs detection has been proposed, overcoming the main drawback of these techniques, i.e., need of knowing: the number of rotor slots R, the position of the RSHs in the spectrum, and their assigned ν index. The algorithm does not use as starting point the RFSHs (avoiding their low accuracy and low detectability for $p = 1$), neither assumes a certain interval for R or erroneously assigns $\nu = 1$ to the highest amplitude RSH, nor uses invasive solutions as no-load test, or inaccurate information, as the rated slip in the nameplate (as previous methods do).

This is the first SSE algorithm that automatically localizes the RSHs family, tracking several RSHs at the same time with one steady state current. It is completely general: works with different skewing angles, and with odd, even or not integer

R/p (since it also detects RSHs with $k > 1$, even if for higher k, the RSHs amplitudes are lower). It precisely estimates the speed with high or low load, grid or frequency converter-fed (high or low fundamental frequency), and high or low slip (specifically tested under the most challenging conditions: low fundamental frequency and low slip).

This is achieved through a new RSHs frequency formula, used by a novel smart search method, which enables to automatically localize and characterize the RSHs (fixing its parameters O_ν and ν), converging when the slip information of the speed-dependent harmonics present in the spectrum (RSHs and up to 16 fault harmonics) matches, thus assuring the accuracy and reliability of the SSE.

The extensive experimental test demonstrates that the SSE algorithm can replace a 1000-line encoder, thanks to its high accuracy: absolute speed error is always below 0.05 rpm and the relative slip error is below 0.5% (0.01 rpm and 0.2% with a frequency converter; error obtained as the average error of 50 tests for each case analyzed). Finally, the field tests show the robustness of the method, since it is proved to work in 100 industrial motors covering all types of rated powers, voltages, speeds, poles pairs, and different operating conditions (21 motors with slips lower than 1%).

Concluding, it is an automatic, non-invasive, accurate, generally applicable and robust speed estimation method for induction motors, which, in addition, can be easily implemented in field monitoring systems due to its low computational burden and simple signal processing. This makes the algorithm a great candidate for use in continuous monitoring systems of motor health and efficiency in industrial environments.

APPENDIX A

Harmonics considered in Section II-B:

$$f_{BBH_1} = (1 \pm k2s)\, f_0 \qquad f_{BBH,2} = \left[\frac{k}{p}(1-s) \pm s\right] f_0$$

$$f_{BBH_{Hilb}} = k2sf_0 \qquad f_{RFSH} = \left[1 \pm k\frac{(1-s)}{p}\right] f_0$$

$$f_{DEH} = \left[\frac{p(O_\nu - \nu) \pm n_D}{p}\,(1-s) + \nu\right] f_0$$

ACKNOWLEDGMENT

This work was supported by the Universitat Politecnica de Valencia and the Spanish Ministry of Science, Innovation and Universities [FPU19/02698].

REFERENCES

[1] J. Hsu, J. Kueck, M. Olszewski, D. Casada, P. Otaduy, and L. Tolbert, "Comparison of induction motor field efficiency evaluation methods," *IEEE Trans. Ind. Appl.*, vol. 34, no. 1, pp. 117–125, 1998.

[2] W. T. Thomson and M. Fenger, "Current signature analysis to detect induction motor faults," *IEEE Trans. Ind. Appl.*, vol. 7, no. 4, pp. 26–34, 2001.

[3] M. Chirindo, M. A. Khan, and P. Barendse, "Analysis of non-intrusive rotor speed estimation techniques for inverter-fed induction motors," *IEEE Trans. Energy Convers.*, vol. 36, no. 1, pp. 338–347, 2021.

[4] J. Bonet-Jara, A. Quijano-Lopez, D. Morinigo-Sotelo, and J. Pons-Llinares, "Sensorless speed estimation for the diagnosis of induction motors via mcsa. Review and commercial devices analysis," *Sensors*, vol. 21, no. 15, 2021.

[5] B. Lu, T. Habetler, and R. Harley, "A survey of efficiency-estimation methods for in-service induction motors," *IEEE Trans. Ind. Appl.*, vol. 42, no. 4, pp. 924–933, 2006.

[6] P. Gangsar and R. Tiwari, "Signal based condition monitoring techniques for fault detection and diagnosis of induction motors: A state-of-the-art review," *Mech. Syst. and Signal. Process*, 2020.

[7] S. H. Kia, H. Henao, and G. Capolino, "Diagnosis of broken-bar fault in induction machines using discrete wavelet transform without slip estimation," *IEEE Trans. Ind. Appl.*, vol. 45, no. 4, pp. 1395–1404, 2009.

[8] H. Guesmi, S. Ben Salem, and K. Bacha, "Smart wireless sensor networks for online faults diagnosis in induction machine," *Computers and Electrical Engineering*, vol. 41, no. 1, pp. 226–239, 2015.

[9] S. B. Lee, D. Hyun, T.-j. Kang, C. Yang, S. Shin, H. Kim, S. Park, T.-S. Kong, and H.-D. Kim, "Identification of false rotor fault indications produced by online mcsa for medium-voltage induction machines," *IEEE Trans. Ind. Appl.*, vol. 52, no. 1, pp. 729–739, 2016.

[10] M. Korzonek, G. Tarchala, and T. Orlowska-Kowalska, "A review on mras-type speed estimators for reliable and efficient induction motor drives," *ISA Trans.*, vol. 93, pp. 1 – 13, 2019.

[11] S. Maiti, V. Verma, C. Chakraborty, and Y. Hori, "An adaptive speed sensorless induction motor drive with artificial neural network for stability enhancement," *IEEE Trans. Ind. Informat.*, vol. 8, no. 4, pp. 757–766, 2012.

[12] S. Das, R. Kumar, and A. Pal, "Mras-based speed estimation of induction motor drive utilizing machines' d- and q-circuit impedances," *IEEE Trans. Ind. Electron.*, vol. 66, no. 6, pp. 4286–4295, 2019.

[13] E. Zerdali, "Adaptive extended kalman filter for speed-sensorless control of induction motors," *IEEE Trans. Energy Convers.*, vol. 34, no. 2, pp. 789–800, 2019.

[14] Jung-Ik Ha and Seung-Ki Sul, "Sensorless field-orientation control of an induction machine by high-frequency signal injection," *IEEE Trans. Ind. Appl.*, vol. 35, no. 1, pp. 45–51, 1999.

[15] J. Holtz, "Sensorless control of induction machines—with or without signal injection?" *IEEE Trans. Ind. Electron.*, vol. 53, no. 1, pp. 7–30, 2006.

[16] T. M. Wolbank, M. A. Vogelsberger, R. Stumberger, S. Mohagheghi, T. G. Habetler, and R. G. Harley, "Autonomous self-commissioning method for speed-sensorless-controlled induction machines," *IEEE Trans. Ind. Appl.*, vol. 46, no. 3, pp. 946–954, 2010.

[17] P. Phumiphak and C. Chat-uthai, "Non-intrusive method for induction motor field efficiency estimation using on-site measurement and modified equivalent circuit," in *2012 15th Int. Conf. on Elect. Mach. and Syst. (ICEMS)*, 2012, pp. 1–5.

[18] A. G. Siraki and P. Pillay, "An in situ efficiency estimation technique for induction machines working with unbalanced supplies," *IEEE Trans. Energy Convers.*, vol. 27, no. 1, pp. 85–95, 2012.

[19] M. Al-Badri, P. Pillay, and P. Angers, "A novel in situ efficiency estimation algorithm for three-phase induction motors operating with distorted unbalanced voltages," *IEEE Trans. Ind. Appl.*, vol. 53, no. 6, pp. 5338–5347, 2017.

[20] A. K. Samanta, A. Naha, A. Routray, and A. K. Deb, "Fast and accurate spectral estimation for online detection of partial broken bar in induction motors," *Mech. Syst. and Signal. Process.*, vol. 98, pp. 63–77, 2018.

[21] PdMA, "Introduction to MCEMAX," [Accessed: 20-10-2021]. [Online]. Available: https://www.pdma.com/PdMA-intro-mcemax.php

[22] Megger, "Instantaneous torque as a predictive maintenance tool for variable frequency drives and line operated motors," [Accessed: 20-10-2021]. [Online]. Available: https://es.megger.com/products/motor-and-generator-testing/dynamic-analyzers/baker-exp4000/technical/instantaneous-torque-as-a-predictive-maintenance-t

[23] M. Ishida and K. Iwata, "A new slip frequncy detector of an induction motor utilizing rotor slot harmonics," *IEEE Trans. Ind. Appl.*, vol. IA-20, no. 3, pp. 575–582, 1984.

[24] A. Bellini *et al.*, "On-field experience with online diagnosis of large induction motors cage failures using mcsa," *IEEE Trans. Ind. Appl.*, vol. 38, no. 4, pp. 1045–1053, 2002.

[25] J. Jung, J. Lee, and B. Kwon, "Online diagnosis of induction motors using mcsa," *IEEE Trans. Ind. Electron.*, vol. 53, no. 6, pp. 1842–1852, 2006.

[26] O. Keysan and H. B. Ertan, "Real-time speed and position estimation using rotor slot harmonics," *IEEE Trans. Ind. Informat.*, vol. 9, no. 2, pp. 899–908, 2013.

[27] U. A. Orji and et al., "Non-intrusive induction motor speed detection," *IET Electric Power Applications*, vol. 9, no. 5, pp. 388–396, 2015.

[28] W. L. Silva, A. M. N. Lima, and A. Oliveira, "Speed estimation of an induction motor operating in the nonstationary mode by using rotor slot

harmonics," *IEEE Trans. Instrum. Meas.*, vol. 64, no. 4, pp. 984–994, 2015.
[29] A. G. Yepes, J. Doval-Gandoy, F. Baneira, and H. A. Toliyat, "Speed estimation based on rotor slot harmonics in multiphase induction machines under open-phase fault," *IEEE Trans. Power Electron.*, vol. 33, no. 9, pp. 7980–7993, 2018.
[30] A. Ferrah, K. G. Bradley, and G. M. Asher, "Sensorless speed detection of inverter fed induction motors using rotor slot harmonics and fast fourier transform," in *PESC '92 Record. 23rd Annual IEEE Power Electron. Spec. Conf.*, 1992, pp. 279–286 vol.1.
[31] R. Blasco-Gimenez, G. M. Asher, M. Sumner, and K. J. Bradley, "Performance of fft-rotor slot harmonic speed detector for sensorless induction motor drives," *IEE Proceedings - Electric Power Applications*, vol. 143, no. 3, pp. 258–268, 1996.
[32] Z. Gao, L. Turner, R. S. Colby, and B. Leprettre, "A frequency demodulation approach to induction motor speed detection," *IEEE Trans. Ind. Appl.*, vol. 47, no. 4, pp. 1632–1642, 2011.
[33] S. Luecke, J. Koupeny, and A. Mertens, "Induction machine speed tracking based on rotor slot harmonics using a modified pll approach," in *2016 18th European Conf. on Power Electron. and Applicat. (EPE'16 ECCE Europe)*, 2016, pp. 1–10.
[34] K. D. Hurst and T. G. Habetler, "Sensorless speed measurement using current harmonic spectral estimation in induction machine drives," *IEEE Trans. Power Electron.*, vol. 11, no. 1, pp. 66–73, 1996.
[35] O. Keysan and H. B. Ertan, "Determination of rotor slot number of an induction motor using an external search coil," *Facta universitatis-series: Electronics and Energetics*, vol. 22, pp. 227–234, 209.
[36] W. J. Bradley, B. Mason, A. Pezouvanis, and K. M. Ebrahimi, "A sensorless speed estimation algorithm for use in induction motor fault detection applications." *Journal of Systems and Control Engineering*, vol. 228, no. 4, pp. 257–264, 2013.
[37] S. Nandi, S. Ahmed, and H. A. Toliyat, "Detection of rotor slot and other eccentricity related harmonics in a three phase induction motor with different rotor cages," *IEEE Trans. Energy Convers.*, vol. 16, no. 3, pp. 253–260, 2001.
[38] S. Nandi, S. Ahmed, H. A. Toliyat, and R. M. Bharadwaj, "Selection criteria of induction machines for speed-sensorless drive applications," *IEEE Trans. Ind. Appl.*, vol. 39, no. 3, pp. 704–712, 2003.
[39] Z. Liu, X. Zhang, X. Yin, and Z. Zhang, "Rotor cage fault diagnosis in induction motors based on spectral analysis of current hilbert modulus," in *IEEE Power Eng. Soc. Gen. Meet, 2004.*, 2004, pp. 1500–1503 Vol.2.
[40] G. Joksimović, E. Levi, A. Kajević, M. Mezzarobba, and A. Tessarolo, "Optimal selection of rotor bar number for minimizing torque and current pulsations due to rotor slot harmonics in three-phase cage induction motors," *IEEE Access*, vol. 8, pp. 228 572–228 585, 2020.
[41] H. W. Penrose, "Appendix5: Stator slot and rotor bar tables," in *Electrical Motor Diagnostics 2nd Edition*. Sucess by Design, 2014.
[42] J. Bonet-Jara, D. Morinigo-SOTELO, O. Duque-Perez, L. Serrano-Iribarnegaray, and J. Pons-Llinares, "End-ring wear in deep well submersible motor pumps," *IEEE Trans. Ind. Appl.*, pp. 1–1, 2022.
[43] C. McClay and S. Williamson, "The variation of cage motor losses with skew," *IEEE Trans. Ind. Appl.*, vol. 36, no. 6, pp. 1563–1570, 2000.

Jorge Bonet-Jara received the M.Sc degree in Industrial Engineering and the Master in Electrical Engineering from the Universitat Politècnica de València (UPV, Spain), in 2016 and 2018, respectively. He is currently carrying out his Ph.D in Fault Diagnosis and Sensorless Speed Estimation in the Electric Engineering Department of the UPV. His research interests include condition monitoring, and modelling of electrical machines.

Joan Pons-Llinares received the M.Sc. degree in Industrial Engineering and the Ph.D. degree in Electrical Engineering from the Universitat Politècnica de València (UPV, Spain), in 2007 and 2013, respectively. He is currently an Associate Professor in the Electric Engineering Department of the UPV. His research interests include time-frequency transforms, condition monitoring and efficiency estimation of electrical machines.